

## Building pH Sensors into Paper-based Small-molecular Logic Systems for Very Simple Detection of Edges of Objects

Jue Ling, Gaowa Naren, Jessica Kelly, Thomas S. Moody and A. Prasanna de Silva

### Supporting Information

#### 1. Synthesis and characterization of **5**

Although close relatives were known<sup>S1</sup> and were available in the laboratory, **5** was prepared since it was expected to cause less problems concerning adequate solubility in aqueous methanol (due to aggregation of these somewhat more hydrophobic relatives).

S1. Daffy, L. M.; de Silva, A. P.; Gunaratne, H. Q. N.; Huber, C.; Lynch, P. L. M.; Werner, T.; Wolfbeis, O. S. *Chem. Eur. J.* **1998**, *4*, 1810-1815.

#### **2,9-Di(2-morpholinoethyl)-1,2,3,8,9,10-hexahydroisoquino[6',5',4':10,5,6]anthra[2,1,9-def]isoquinoline-1,3,8,10-tetraone (5)**

Perylenetetracarboxylic-3,4,9,10-bisanhydride (2.0 g, 5.0 mmol), dicyclohexylcarbodiimide (DCC) (0.7 g, 3.4 mmol) and 4-(2-aminoethyl) morpholine (2.60 g, 20 mmol) were refluxed with vigorous stirring in an inert atmosphere at 240 C for 4 hours in quinoline (15 mL). After cooling to room temperature, the reaction mixture was poured into ethanol (200 mL) and the precipitate filtered and dried. This gave a black solid (1.97 g, 69%).

Melting point = >400 C

Found:	C <sub>36</sub> H <sub>32</sub> N <sub>4</sub> O <sub>6</sub>	C, 70.04; H, 4.90; N, 9.20.
Required for	C <sub>36</sub> H <sub>32</sub> N <sub>4</sub> O <sub>6</sub>	C, 70.12; H, 5.23; N, 9.09.

<sup>1</sup>H NMR (CDCl<sub>3</sub>) 500 MHz      δ8.70(d, 4H, ArH, J=7.9 Hz), 8.65(d, 4H, ArH, J=7.9 Hz), 4.38(t, 4H, C(=O)NCH<sub>2</sub>, J=7.2 Hz), 3.69(t, 8H, N(CH<sub>2</sub>CH<sub>2</sub>)<sub>2</sub>O, J=4.5 Hz), 2.75(t, 4H, C(=O)NCH<sub>2</sub>CH<sub>2</sub>, J=7.5 Hz), 2.62(bt, 8H, N(CH<sub>2</sub>CH<sub>2</sub>)<sub>2</sub>O).

<sup>13</sup>C NMR (CDCl<sub>3</sub>) 125 MHz      δ164, 132, 129, 125, 124, 67, 56, 54, 53, 36.

i.r. (ν<sub>max</sub>) KBr:      3435, 2960, 2852, 1691, 1650, 1438, 1358, 811 cm<sup>-1</sup>.

m/z(%), (E.I.): 617(10, M<sup>+</sup>+1), 567(8), 499(10), 431(18),  
399(20), 363(25), 310(35), 301(68), 281(48),  
266(50), 252(32), 236(42), 227(100).

Fluorescence emission spectra of **5** as a function of pH.

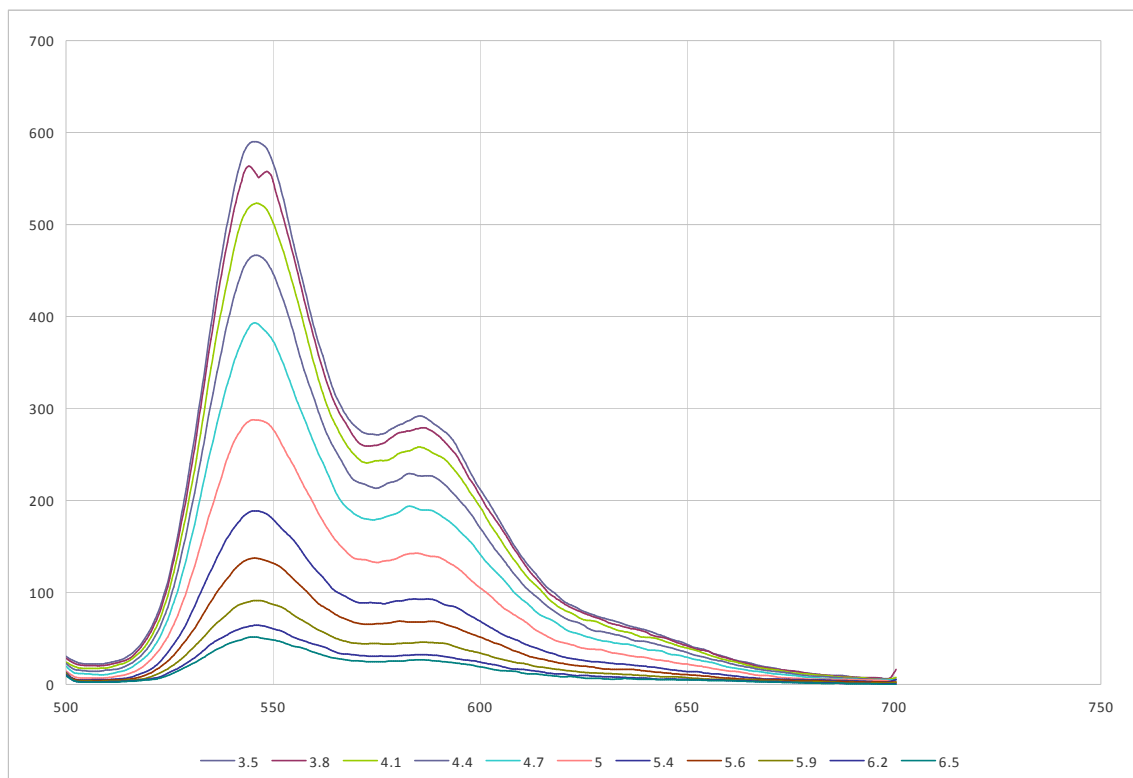


Figure S1. Fluorescence emission spectra of **5** as a function of pH in methanol: water (1:1, v/v) (excited at 492 nm). The y-axis is fluorescence intensity (a.u.) and the x-axis is wavelength (nm). The pH values are stated below the spectra.

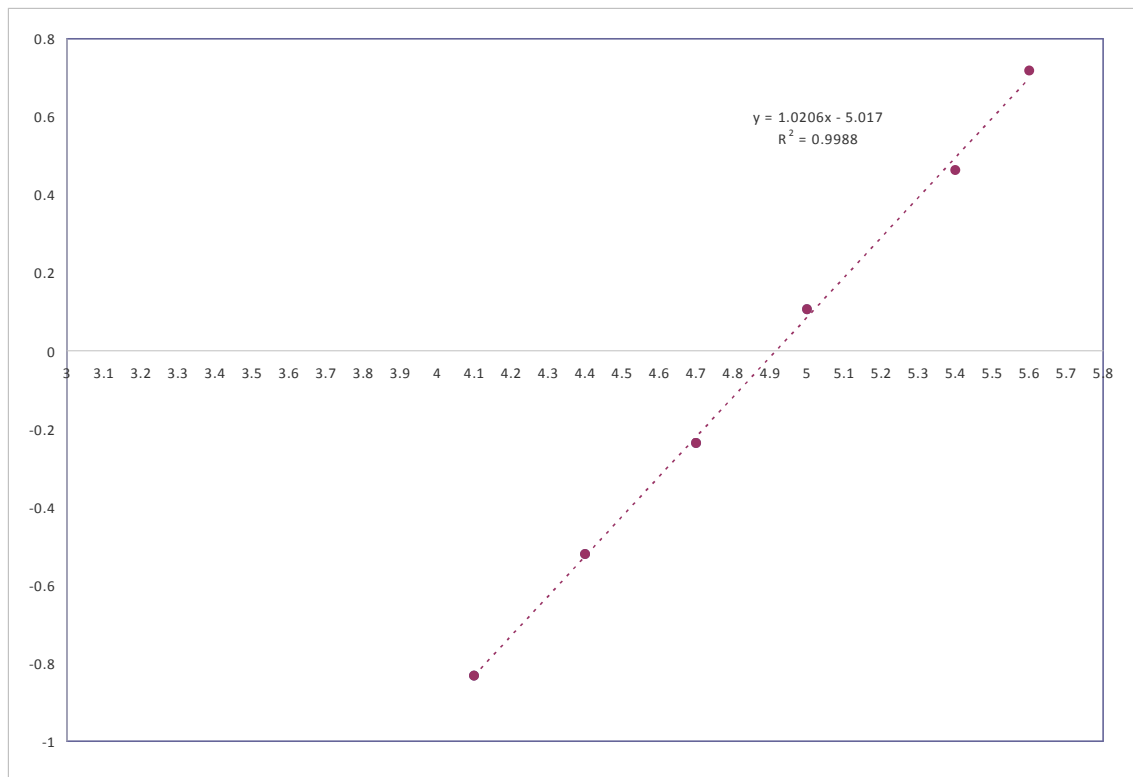


Figure S2. Henderson-Hasselbalch plot according to the equation<sup>S2</sup>:  $\log[(I_{Fmax} - I_F)/(I_F - I_{Fmin})] = \text{pH} - \text{pK}_a$ . The y-axis is  $\log[(I_{Fmax} - I_F)/(I_F - I_{Fmin})]$  where  $I_F$  is fluorescence intensity at 545 nm and the x-axis is pH. The x-axis intercept delivers the  $\text{pK}_a$  value as 4.9.

S2. Bissell, R. A.; Calle, E.; de Silva, A. P.; de Silva, S. A.; Gunaratne, H. Q. N.; Habib-Jiwan, J. -L.; Peiris, S. L. A.; Rupasinghe, R. A. D. D.; Samarasinghe, T. K. S. D.; Sandanayake, K. R. A. S.; Soumillion, J. -P. *J. Chem. Soc. Perkin Trans. 2* **1992**, 1559-1564.

## 2. Ferrioxalate actinometry

Ferrioxalate actinometry for the cuvet experiment was carried out according to the procedure in ref S3.

S3. Montalti, M.; Credi, A.; Prodi, L.; Gandolfi, M.T. *Handbook of Photochemistry* 3rd Ed., CRC Press, Boca Raton, **2006**.

Ferrioxalate actinometry for the filter paper experiment was carried out according to a modification of the procedure in ref S3.

The filter paper was soaked for 10 minutes in a 0.012 M potassium ferrioxalate solution in 0.05 M  $\text{H}_2\text{SO}_4$  in the dark. Then the paper was drained of excess liquid as usual and laid in the center of the glass plate. Then the full paper was exposed (without a mask) to 254 nm radiation as usual for a chosen time period. Then the filter paper and the contacted area of the glass plate were washed with

portions of 0.05 M H<sub>2</sub>SO<sub>4</sub> through a glass funnel and the volume of the washings made up to 30 ml in a flask covered with silver foil. Then 5.0 mL of buffered phenanthroline solution was added and the absorbance at 510 nm measured immediately.

We note that actinometry on the filter paper can only give approximate values for the photon flux due to competitive scattering and absorption from the paper fibres. For the purpose of the flux calculation, we make the assumption that the stained paper is absorbing all the incident radiation. The photon fluxes for the solution studies are more reliable.

3. Estimation of the number of molecules involved in producing the edge of the 'square' object.

From the uv spectra of the exhaustive extract from the substrate (at zero exposure time)(Figure 2b), we note that the absorbance at 411 nm in a 1 cm cuvet is 0.115. Since the molar absorption coefficient ( $\epsilon$ ) of **1** at 411 nm is 20,000,<sup>21</sup> the concentration of **1** in the extract is  $5.8 \times 10^{-6}$  M according to the Beer-Lambert equation. Since the total volume of the extract is 50 mL, the total number of molecules of **1** is  $1.75 \times 10^{17}$ . These are distributed over the surface area of the filter paper [ $\pi(11.0/2)^2 = 95 \text{ cm}^2$ ]. The object 'square' has sides of length 4.1 cm. The image has a sharpest edge thickness of 1 mm. So the area producing the essential edge detection is a square of sides of 4.2 cm =  $17.6 \text{ cm}^2$ . So the number of molecules of **1** available in this area is  $(17.6/95) \times 1.75 \times 10^{17} = 3.2 \times 10^{16}$ .

4. Justification of the PET basis of the bimolecular fluorescent quenching processes with electrochemical data on **2**, **3** and **4**.

$E_{\text{reduction}}$  of **2** is  $-1.5 \text{ V}^{\text{S4}}$  (reference: standard calomel electrode in all cases).

Ref 24 cites  $E_{\text{oxidation}}$  of diphenylsulfide as  $+1.4 \text{ V}$ . Compound **3**, being a phenyl substituted diphenylsulfide (albeit at the 2-position), would have a significantly lower  $E_{\text{oxidation}}$  value.

$E_{\text{reduction}}$  of **4** is  $-1.6 \text{ V}^{\text{S5}}$  and  $E_{\text{oxidation}}$  of **4** is  $+1.1 \text{ V}^{\text{S5}}$ .

So we see, by comparing their  $E_{\text{reduction}}$  values, that the thermodynamic driving force for PET from **4** to **2** is exergonic by 0.1 eV. While electrochemical data for **1** are not available, its structural closeness with **4** suggests that the  $K_{\text{SV}}$  value of  $96 \text{ M}^{-1}$  (for the bimolecular quenching of the fluorescence of protonated **1** by **2** via PET from **1** to **2**) is understandable in this way.

Radical ion pairing makes PET processes between neutral species more exergonic by  $0.1 \text{ eV}^{\text{S6}}$ . So we can understand, by comparing their  $E_{\text{oxidation}}$  values and by allowing for the radical ion pairing, that the thermodynamic driving force

for PET from **3** to **4** is probably isoergonic or even exergonic. Hence the  $K_{SV}$  value of  $110 \text{ M}^{-1}$  (for the bimolecular quenching of the fluorescence of protonated **1** by **3** via PET from **3** to **1**) is understandable as before.

S4. Vase, K. H.; Holm, A. H.; Norrman, K.; Pedersen, S. U.; Daasbjerg, K. *Langmuir* **2008**, *24*, 182-188.

S5. de Silva, A. P.; Gunaratne, H. Q. N.; Habib-Jiwan, J. -L.; McCoy, C. P.; Rice, T. E.; Soumillion, J. -P. *Angew. Chem. Int. Ed. Engl.* **1995**, *34*, 1728-1731.

S6. Grabowski, Z. R.; Dobkowski, J. *Pure Appl. Chem.* **1983**, *55*, 245-252.

##### 5. The influence of drying on the clarity of edge detection.

Figure S3 shows that no drying causes convective diffusion of the aqueous methanol within the filter paper pores and channels. This leads to fast spreading of  $\text{H}^+$  (which gives fluorescence switching 'on' of the sensor molecules) from the irradiated 'square' area to cover the entire filter paper via convective diffusion. The slower-diffusing quencher 2-(phenylthio)biphenyl (which is the photoproduct accompanying  $\text{H}^+$ ) causes the ill-defined dark square at 32 min exposure.

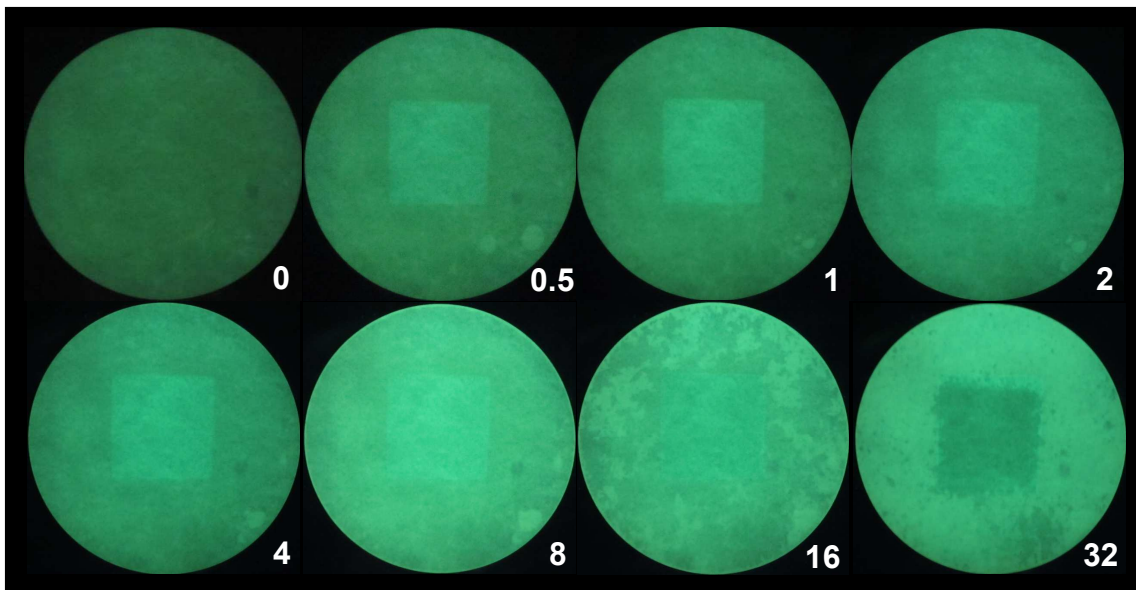


Figure S3. Photographs of fluorescent images after 254 nm writing light is shone through the 'square' mask onto the substrate, containing the logical molecular solution including **1** (as in Figure 2a) but without drying, for varying time periods.

Figure S4 shows that too much drying (for 10 minutes) gives only the faintest (albeit sharp) edge development and Figure S5 shows that even longer drying (for 20 minutes) gives no edge development at all, though excellent 'positive photographs' are produced at short exposure times. These longer drying times also give rise to some aggregation of the unprotonated sensor molecules on the filter paper, which leads to red-shifting of the fluorescence from green to yellow.

However, the protonated sensor molecules de-aggregate and show up as blue-green emission in Figure S5.

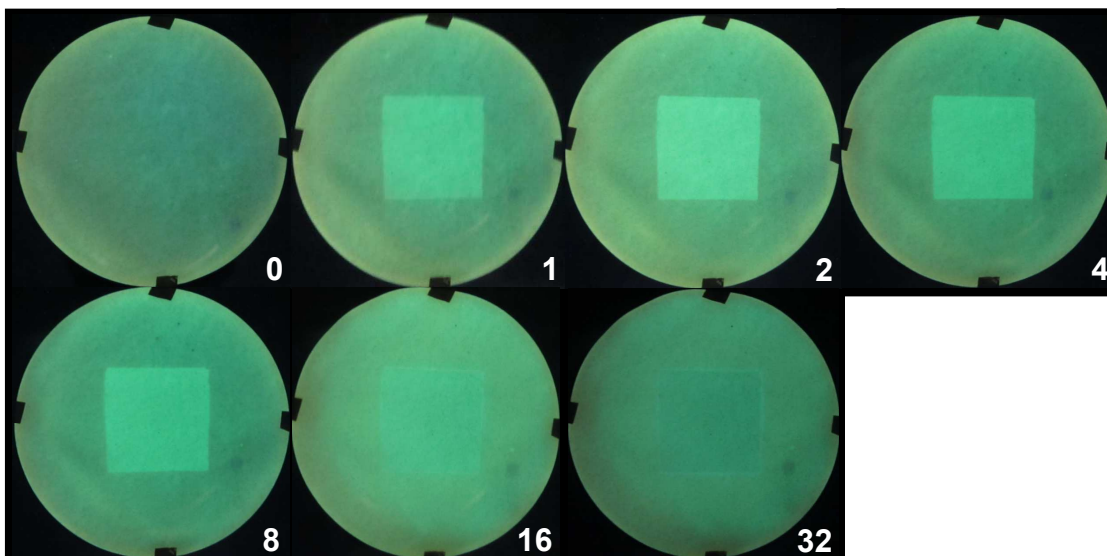


Figure S4. Photographs of fluorescent images after 254 nm writing light is shone through the 'square' mask onto the substrate, containing the logical molecular solution including **1** (as in Figure 2a) but with drying for 10 min, for varying time periods. The filter paper is too dry to stick to the backing glass plate to maintain registration during multiple 'writing/mask removal/reading/mask replacement' cycles. So the filter paper is stuck down on the glass plate with four pieces of tape.

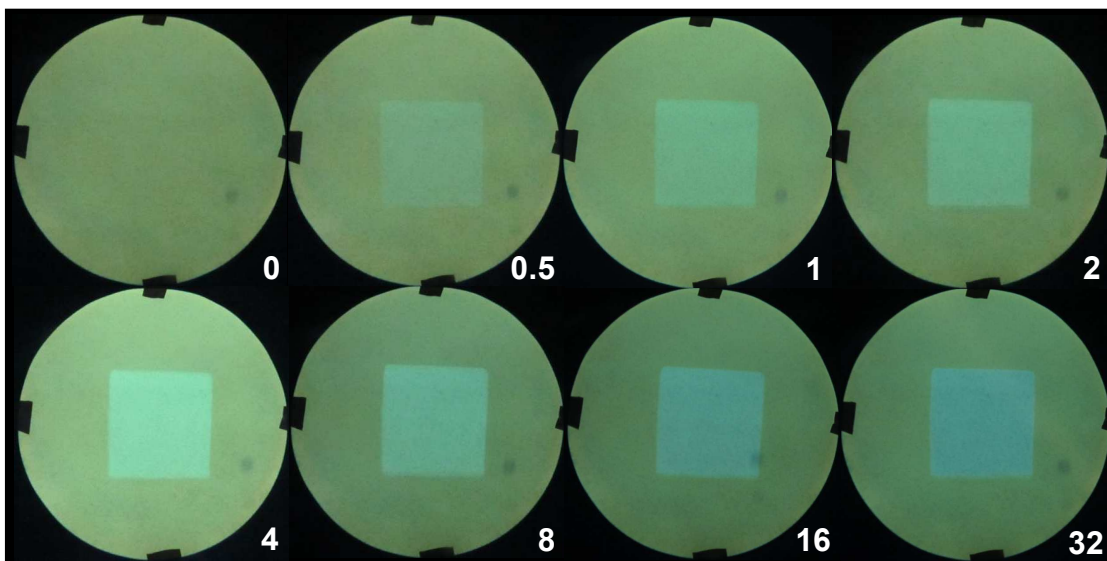


Figure S5. Photographs of fluorescent images after 254 nm writing light is shone through the 'square' mask onto the substrate, containing the logical molecular

solution including **1** (as in Figure S4) but with drying for 20 min, for varying time periods.

#### 6. Elimination of possible contact effects by using a spacer mask.

The configuration of the masks are shown in Figure S6. The resulting photograph is in Figure S7, which shows the edge detection is preserved except for the slight loss of focus due to the separation of the mask from the substrate.

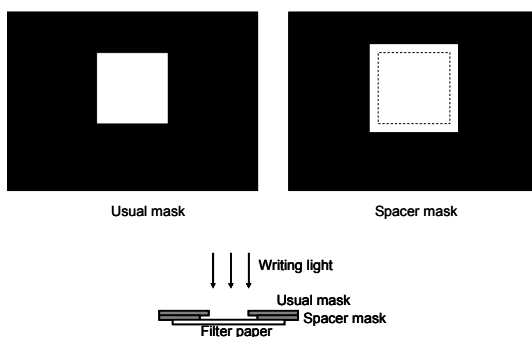


Figure S6. Schematic of the spacer mask experiment (not to scale)

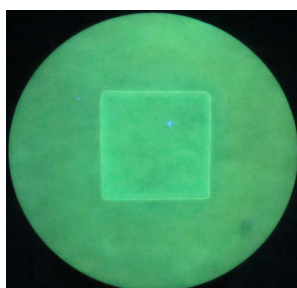


Figure S7. Except for the spacer mask, the other conditions are those used for **1** with a single exposure of 32 min (as in Figure 1).

#### 7. The smallness of the molecules employed in this work

Ref. 9 elegantly showed that a carefully choreographed reactive network of large biomolecules (approximate total molecular mass  $9020+24543+16606+9246+6278=65693$ ) could achieve edge detection. Many life processes are based on reactive networks of large biomolecules with high levels of organization in space/time. Our synthetic molecules are as small as, total molecular mass  $350+299+106=755$  in the case of **4**, photo acid generator and buffer. These are 90-fold smaller than the biomolecules. Our small synthetic molecules have no organization which is relevant to life, except being spread out on paper to create

the graphical interface, and they still achieve information processing that is a deep aspect within our human nature.

#### 8. Experimental details pertinent to Figure 1.

The object is a hole cut in an opaque, rigid plastic mask, e.g. 'square' and 'star' in order of increasing complexity. The objects are backlit for photography. The writing light is 254 nm radiation from a common laboratory ultraviolet lamp assembly (Camag). This is shone through the mask onto the substrate for the optimum time period, which is 30, 16 and 32 min for fluorescent sensors **1**, **4** and **5** respectively. The reading light is 366 nm radiation from the same ultraviolet lamp assembly. Reading is done visually or with a camera (Canon IXUS 115HS), after removal of the mask. The latter are the fluorescent images shown. The substrate is a common laboratory filter paper circle (Whatman 1004 110, 11.0 cm diameter, 0.2 mm thickness) soaked in the logical molecular solution for 10 min, drained of excess liquid, laid on a glass plate, kept at 50 C for 4 min and then placed under the lamp (254 nm light intensity =  $3.4 \times 10^{-9}$  Einstein  $\text{cm}^{-2} \text{min}^{-1}$ ). The logical molecular solution is composed of  $10^{-4}$  M sensor (**1**, **4** or **5**) and  $10^{-3}$  M **2** in methanol: water (1:1, v/v) with  $10^{-4}$  M  $\text{Na}_2\text{CO}_3$  adjusted to pH 9.2. This pH value is chosen to be >1 unit greater than the  $\text{pK}_a$  value of the sensor, which is 7.3,<sup>38</sup> 7.2<sup>38</sup> and 4.9 for **1**, **4** and **5** respectively. The blue emission seen during experiments with **5** is due the background fluorescence of the filter paper when it is soaked in the solution of **2**. Because compound **5** is not very soluble, it adsorbs strongly on the paper and thus behaves very well as an edge detector by showing hardly any residual convective diffusion.

#### 9. Experimental details pertinent to Figure 2.

a) Photographs of fluorescent images after 254 nm writing light is shone through the 'square' mask onto the substrate, containing the logical molecular solution including **1**, for varying time periods. The cumulative time in minutes is noted in each photograph. b) Uv spectra of the exhaustive extract from the substrate, containing the logical molecular solution including **1**, after exposure to 254 nm writing light for 0 and 32 min respectively. The extract was made with methanol: water (1:1, v/v) at pH 3.0 and made up to a total volume of 50 mL. **2** absorbs most of the 254 nm writing light but is transparent to the 366 nm reading light.<sup>44</sup> The blue line shows that **1** is largely preserved during irradiation, whereas **2** is significantly decomposed (into **3** and  $\text{H}^+$ ).<sup>44</sup> c) Fluorescence emission spectra (excited at 366 nm) of the logical molecular solution including **1**, while it is irradiated with 254 nm light (flux =  $6.9 \times 10^{-8}$  Einstein  $\text{min}^{-1}$ ) for the stated cumulative times in minutes. This experiment is conducted in a cuvet with 3 mL of solution. The emission in the 400-450 nm region is due to the photoproduct **3**. Inset: Temporal variation of fluorescence intensity (emitted at 504 nm) abstracted from the fluorescence spectra.

#### 10. Experimental details pertinent to Figure 3.

Photographs of fluorescent images after 254 nm writing light is shone through the 'square' mask onto the substrate, containing the logical molecular solution including **5**, for varying time periods. The cumulative time in minutes is noted in each photograph. Only the zoomed-in sections of the irradiated region and the adjacent areas are shown.

#### 11. Additional information for Figure 4.

Scheme of visible edge development. Proton Concentration – distance profile at time = 0 (red). Proton Concentration – distance profile at time = t (blue), since protons have diffused according to Fick's laws. Concentration of **3** – distance profile at time = t (green), since the quencher product diffuses far slower. Concentration of **3** – distance profile at time = 0 is not shown for clarity, but it is similar to the red curve for protons. The visible edge appears in the unirradiated region adjacent to the mask boundary where **3** has not arrived yet (due to slow diffusion) and where the protons have arrived (due to faster diffusion) in sufficient numbers to overwhelm the local sodium carbonate buffer. The two points where the horizontal pink line intersects the blue curve shows where the protons (which have arrived in the locality) have exactly cancelled out the local buffer. At points further away from the center of the irradiated area, the basic buffer still rules and therefore the fluorescence remains switched 'off'. The observed edges are shown in black.